

An Efficient Glucose Biosensor Based on TiO₂ Hollow Sphere Prepared via a Carbon-Sphere Template Method

Xingrui Zheng¹, Song Lv¹, Zhentao Yuan¹, Yao Liang^{1*}, Yan Wei², Hongzhong Cai²

¹ City college, Kunming University of Science and Technology, Kunming 650500, China

² State Key Laboratory of Advanced Technologies for Comprehensive Utilization of Platinum Metals, Kunming Institute of Precious Metals, Kunming 650106, China

*E-mail: kmust_ly@126.com

Received: 6 November 2019 / Accepted: 14 January 2020 / Published: 10 February 2020

A glucose biosensor based on hollow sphere TiO₂ was prepared via a simple synthesized method that used carbonaceous spheres as template. The studies indicated that the glucose biosensor based on hollow sphere TiO₂ is characterized to high surface area, narrow pore size distribution as well as the high sensitivity of 5.64 mA M⁻¹cm⁻¹, which facilitates the direct electron transfer between glucose oxidase (GO_x) and surface of electrodes. Most importantly, this material display long-time stability and reproducibility and achieved 94% stable current only with 3s. Meanwhile, it still maintains the 70% of current response after two months later, indicating that the hollow sphere TiO₂ prepared via a carbon-sphere template method is a promising material for the construction of glucose biosensor and other biologic applications.

Keywords: Hollow sphere TiO₂; glucose biosensor; carbonaceous sphere; glucose oxidase

1. INTRODUCTION

The fast and accurate detection of physiological glucose and direct electron transfer (DET) between protein and an electrode are of great crucial to constructing high-performance glucose biosensor [1-3]. However, the redox center of enzyme is seated in an isolated protein hull, which leads to the DET of enzyme is difficult to observe at traditional electrodes [4,5]; for example, the prosthetic group of glucose oxidase (GO_x) located in the inner of insulating protein shell around 13Å that surpasses usually the electron-tunneling distance. Therefore, the redox mediators have been employed to accelerate electron transfer between flavin group (FAD) redox center of GO_x and the surface of electrodes [6,7]. Over the past decades, a variety of nanomaterials with unique physical and electrical performance have widely been explored for constructing glucose biosensors since nanomaterials can availably shorten electron-tunneling function and improve the DET capability of electrodes [8,9], such

as metal oxides [10], nanomaterials composed of carbon [11]. Actually, the weak biocompatibility of these nanomaterials is difficult to maintain the activity of enzymes, limiting their practical applications.

In recent years, the diverse nanostructures of TiO₂ materials have been widely studied and used in many fields including solar cells [12], electrochromic devices [13] and lithium-ion batteries [14], attributing to its outstanding photocatalytic performance and outstanding electron-transfer behavior. In addition, TiO₂ nanomaterials have also been introduced to improve proteins and enzymes immobilization for glucose biosensor as its excellent biocompatibility, chemical and thermal stability [15,16]. Furthermore, it is noticeable that the electrochemical property of glucose biosensors is affected not only by its crystalline structure, but also influenced by its dimension, the surface area of materials as well as geometry. It is well known that the quantum confinement effect and electron transport performance of TiO₂ nanomaterials generally controlled by its size and geometry [17,18]. Therefore, TiO₂ with different sizes and morphology was synthesized for developing high-performance biosensors, such as new nanostructured TiO₂ [19], tetragonal columnar-shaped TiO₂ nanorods [20] and TiO₂ nanowire [21]. All of those materials display the excellent performance for fabricated biosensors due to their high surface area and uniform pore distribution that provides more active sites for enzyme absorbed.

The template-assisted preparation methods are always introduced to making all kinds of nanostructures by using different templates, including porous anodic alumina [22], polystyrene spheres [23] for it is character to simplicity and low-cost. In this work, hollow spheres TiO₂ was synthesized by sol-gel method and used carbonaceous spheres (C spheres) as a template. The synthesized hollow spheres TiO₂ possess high surface area and narrow distribution of pore sizes that is to the benefit of adsorbing GOx and the fabricated glucose biosensor based on hollow spheres TiO₂ shows excellent electrocatalytic activity, selectivity as well as long-time stability.

2. MATERIALS AND METHODS

2.1 Reagents and apparatus

GOx and pure titanium were purchased from Sigma. Ascorbic acid (AA), L-cysteine (L-Cys) and urea were supplied by Alfa Aesar. Phosphate buffer saline (PBS) was obtained from reactivity of between NaH₂HPO₄ and Na₂HPO₄.

Morphological characterization and microstructure were examined by SEM (JSM-6700F), TEM (Tecnai G2 20) as well as XRD (Bruker AXS X-ray diffractometer). The specific surface area was measured by using a BET analyzer and pore size distribution was calculated by the Barrett-Joyner-Halenda(BJH). Fourier transform infrared measurements(FT-IR) were performed on a Bruker EQUINOX 55 duoscope to confirming the activity of enzymes. All electrochemical measurements were tested on CHI 760B electrochemical workstation. A three-electrode system was used with the prepared TiO₂ modified GCE or bare GCE as the working electrode and a platinum wire as the auxiliary electrode, a Ag/AgCl (saturated KCl) as the reference electrode. Electrochemical impedance spectroscopy (EIS) was performed in 0.1 M KCl solution containing 5 mM Fe(CN)₆^{3-/4-} (1:1) as a

supporting electrolyte at its open circuit potential with a frequency range from 1.0×10^{-2} to 1.0×10^5 Hz, using an alternating current voltage of 5 mV.

2.2 Preparation of hollow spheres TiO_2

The synthesized method of hollow sphere TiO_2 is simple by using C spheres as a template. Firstly, 6 ml $Ti(OC_4H_9)_4$ was dispersed into 30 ml ethanol solution and stirring successively during the process of forming a characteristic solution. Secondly, the C spheres that was fabricated by a hydrothermal method were added to the as-prepared mixed solution above, followed by keeping at room temperature for 20 hours with vigorous stirring and finally were collected by centrifugation, which can be obtained the stable C@ TiO_2 shell structure. To remove the residual cations and anions, the obtained TiO_2 samples were washed with ethanol repeatedly and then dried in air at 50°C. Finally, the anticipative hollow hollow spheres TiO_2 were achieved by annealing at 500°C for 3 hours to remove the C spheres.

2.3 Preparation of TiO_2 modified electrodes

Firstly, glassy carbon electrodes (GCE) was polished by using alumina slurry of 0.3 mm, followed by rinsing with distilled water. Meanwhile, the GCE was sonicated in a 1:1 solution of nitric acid and acetone in doubly distilled water to ensuring the purity of electrode surface. Secondly, the GO_X immobilized to electrodes can be obtained by dispersing as-prepared samples (25 mg TiO_2 hollow spheres) into solution containing 30 μL of Nafion and 250 μL of distilled water. After dissolving sufficiently, the mixed solution was dipped on to the surface of bare GCE and dried at 27°C for 20 hours. Finally, the TiO_2 /GCE electrode was dipped into the GO_X solution of 5 μL and dried at 27°C for 20 hours. In the end, the GO_X - TiO_2 /GCE electrodes was cleaned by ultra-pure water and stored it under the environment of 4°C.

3. RESULTS AND DISCUSSION

3.1 Material characterization

Fig.1 displays the morphology and crystal structure of fabricated TiO_2 . As shown in Fig.1A, the SEM image depicts the surface morphology of as-prepared TiO_2 and anticipative spherical structures could be distantly observed. The SEM images with high magnification shown in Fig.1B revealed that the samples consist of occasional broken TiO_2 spheres, which is beneficial for adsorbing enzymes into the inner of hollow spheres TiO_2 for it provided more active sites. The TEM image shown in Fig.1C displays that TiO_2 possess a hollow structure and the size of the TiO_2 hollow spheres is about the 400-600 nm. The thickness of TiO_2 hollow spheres is about range from 30 to 35 nm, which is beneficial to accelerate electron transfer from immobilized protein to the electrode surface. Fig.1D depicts the XRD pattern of as-synthesized TiO_2 crystal structure, the main peaks at 25.3°, 37.7°, 48.0°,

53.8° , 55.0° and 62.1° is agreement with the (101), (004), (200), (105), (211), and (204) of pure anatase phase (JCPDS card 65-5714). No other peaks were discovered from XRD patterns, confirming that the high purity and well crystallinity of the prepared samples.

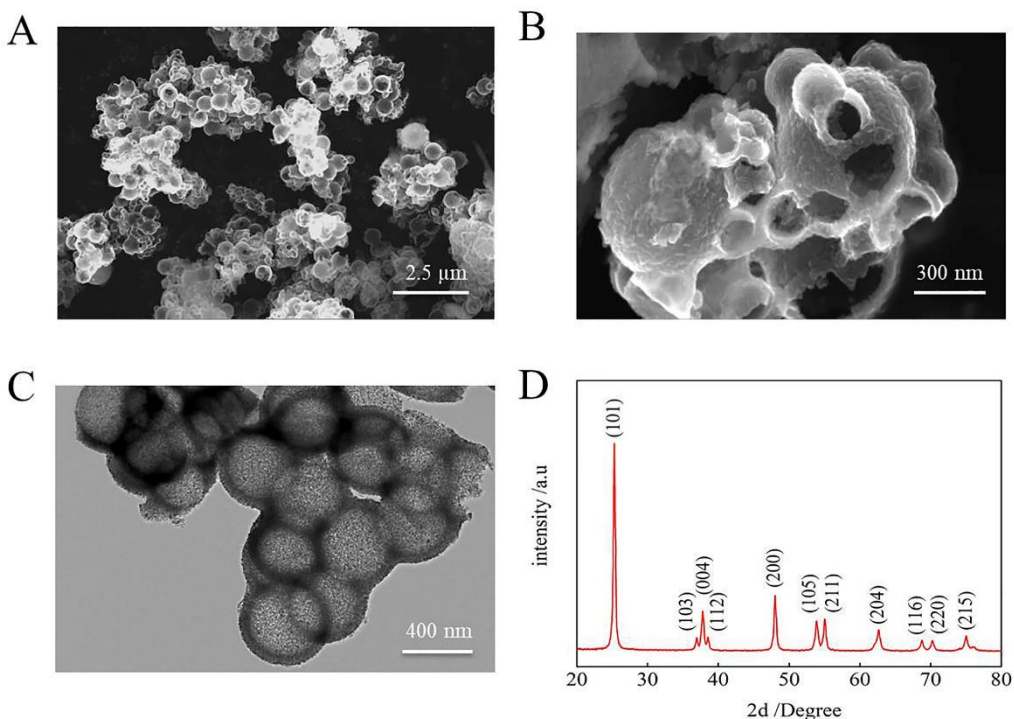


Figure 1. (A) low and (B) high magnification images of TiO_2 spheres, (C) TEM spectrum of the prepared TiO_2 hollow spheres material, (D) XRD patterns of the prepared materials.

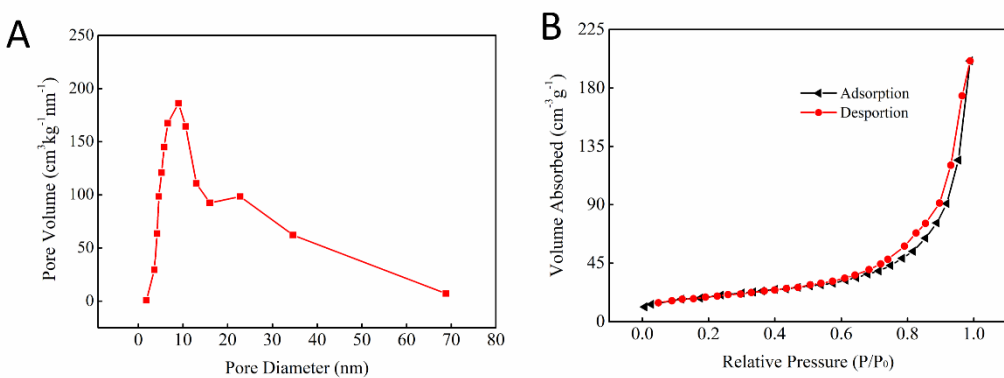


Figure 2. (A) nitrogen adsorption-desorption isotherms of TiO_2 hollow spheres and (B) pore size distribution of prepared TiO_2

The nitrogen-desorption isotherm and Barrett-Joyner-Halenda have been used to investigate the mesoporous and pore-size distribution of prepared TiO_2 sample. It is can be seen from Fig.2A that the hollow spheres TiO_2 exhibits type-IV isotherm showing a hysteresis loop at the high relative pressure (P/P_0), which indicates the presence of porous inside TiO_2 spheres. The specific surface area of TiO_2 spheres were calculated to be $128.6 \text{ m}^2 \text{g}^{-1}$ by Brunauer Emmett Teller method. Such a high surface

area is mainly due to its unique mesoporous structure. From the pore-sized distribution curve depicted in Fig.2B, the TiO_2 spheres possesses uniform porous distribution and the pore diameter is dominant in the range from 7 to 12 nm that is favorable to the GO_X molecules enter the inner pores of TiO_2 spheres. Therefore, the TiO_2 hollow spheres were beneficial for GO_X immobilization and is expect to be promising nanomaterials to the construction of biosensor for its high surface area and uniform pores distribution.

3.2 Immobilization of GO_X on TiO_2

As known from results above, the fabricated hollow spheres TiO_2 were beneficial to enzyme absorption on the electrode. Hence, in order to investigate the activity of immobilized GO_X , the FT-IR was employed to detecting the secondary structure changes of GO_X was immobilized on modified electrodes. The FT-IR spectra of bare GC, TiO_2 - GO_X and TiO_2 were shown in Fig.3A. From FT-IR spectrum of GO_X sample, two typical absorption bands were observed at 1658 and 1545 cm^{-1} , consisting with the typical amide I and II absorption of proteins respectively, which was widely seen as the denaturation and conformational change upon proteins [24]. Another characteristic peak centered at 1100 cm^{-1} can be obtained that was ascribed to the C-O stretching vibration of GO_X . Meanwhile, it is clear observed that Adsorption peaks of amide I band and amide II band presence in the FT-IR spectrum of GO_X/TiO_2 , indicating the GO_X has been successfully immobilized on the surface of TiO_2 hollow spheres and still retain its bioactivity. moreover, the adsorption peak has shifted mildly, which can be accounted for the electrostatic interaction of GO_X and TiO_2 hollow spheres, moreover, TiO_2 have grater isoelectric point in comparation with the that of GO_X in a neutral solution (isoelectric point =4.2)[25].

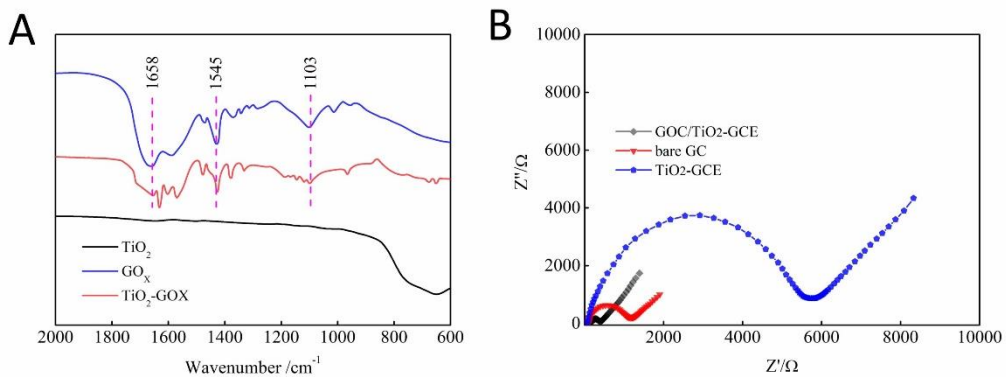


Figure 3 (A) FT-IR spectra of TiO_2 , GO_X , TiO_2 - GO_X as well as GO_X .(B) Nyquist plots of bare GCE, TiO_2 -GCE and GO_X/TiO_2 -GCE electrodes respectively.

The EIS technique is extensively used to investigate the interface property of electrode. The Nyquist plots of three different electrodes shown in Fig.3B, the GO_X - TiO_2 modified electrode displayed a greater electron transfer resistance rather than GCE and TiO_2 -GCE electrodes because the GO_X possess so low electroconductibility that resist the electron transfer on the surface of electrodes, indicating that the GO_X has been adsorbed to the TiO_2 -GCE electrodes. The result is the same as the

Fig.3A. Moreover, the surface coverage (θ) of GO_X on hollow sphere TiO_2 was also calculated from Nyquist plots [26]. The calculated θ was 85.4% according to the equation: $\theta = 1 - R_{ct}/R_{ct}^{GO_X}$, where the R_{ct} and $R_{ct}^{GO_X}$ represents the value of resistance in term of TiO_2 -GCE electrode as well as GO_X - TiO_2 modified electrode respectively. The high surface coverage of GO_X mainly attribute to its large adsorption sites and hollow nanostructure.

3.3 Direct electrochemistry of $GO_X/TiO_2/GCE$

It is well-known that cyclic voltammetry (CV) can be used to measure electron transfer behavior between protein and electrode surface. Fig.4A shows CV plots of the different modified GCE electrodes, which was measured in N_2 -saturated PBS solution with the scan rate of $100 mV s^{-1}$ ($pH=7.0$). It is can be seen from the CV of GO_X - TiO_2 /GCE that there exists a pair of well-defined peaks with anodic (E_{Pa}) and cathodic (E_{Pc}) at -0.404 and -0.446 V respectively, corresponding to the typical electrochemical characteristics of GO_X and caused by the reversible reaction as : $FAD + 2H^+ + 2e \leftrightarrow FADH_2$. Meanwhile, the peak separation ($\Delta E_P = E_{Pa} - E_{Pc}$) was around 42mV, much lower than that of other TiO_2 nanostructure, for example, the mesoporous TiO_2 [27] (58mV), confirming that the fabricated hollow spheres TiO_2 possesses more excellent electron transfer rate and offered great advantages to construct glucose biosensor. In addition, no typical peaks were observed from the CV curve of TiO_2 /GCE and bare GCE, indicating that only the presence of GO_X was indispensable to current response.

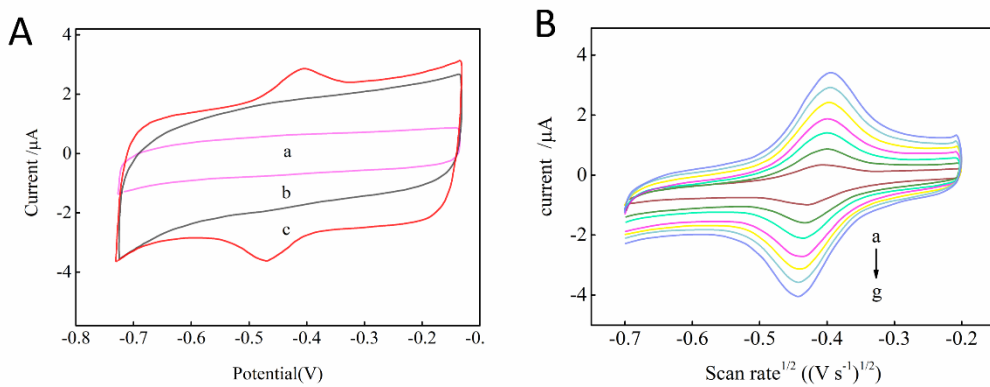


Figure 4 (A) Cyclic voltammograms of the modified electrodes in 0.1M nitrogen-saturated PBS solution at $100 mV s^{-1}$ ($pH=7.0$). (a) bare GCE, (b) TiO_2 -GCE, (c) GO_X / TiO_2 -GCE. (B) CVs of GO_X / TiO_2 -GCE in 0.1M pH 7.0 O_2 -saturated at different scan rates (100 - 700 $mV s^{-1}$ from a to g).

Based on the Laviron theory [28], electron transfer rate constant (k_s) can be obtained from the CV curve at high scan rate following the equation: $k_s = mnFV/RTk$, where n , F , V represents electron transfer number ($n = 2$), faraday constant as well as the scan rate respectively, R is the gas constant, T is the temperature and m is the constant associated with ΔE_P . The k_s of GO_X - TiO_2 /GCE was calculated to be $7.2 s^{-1}$ from CV plot, which is greater than that of GO_X absorbed on other

nanomaterials, for example, MWCNTs (1.12 s^{-1}) [29] SWCNTs (0.3 s^{-1})[30] and Au nanoparticles (2.2 s^{-1})[31].

The result demonstrated the excellent DET of TiO_2 hollow spheres immobilized GO_X . As shown as Fig.4B, the influence of scan rate for electrochemical response was investigated from 100 to 700 mV s^{-1} and the current response raise along with the increase of scan rate, which confirmed that the GO_X redox reaction is a surface-controlled electrochemical process [32,33]. The separation between anodic peak and cathodic peak raise similarly along with the increase of scan rate owing to the resistance of modified layer. Therefore, the TiO_2 hollow spheres can be regarded as ideal materials for biosensors because of its excellent electron transfer [34].

3.4 Glucose biosensor performance characterization

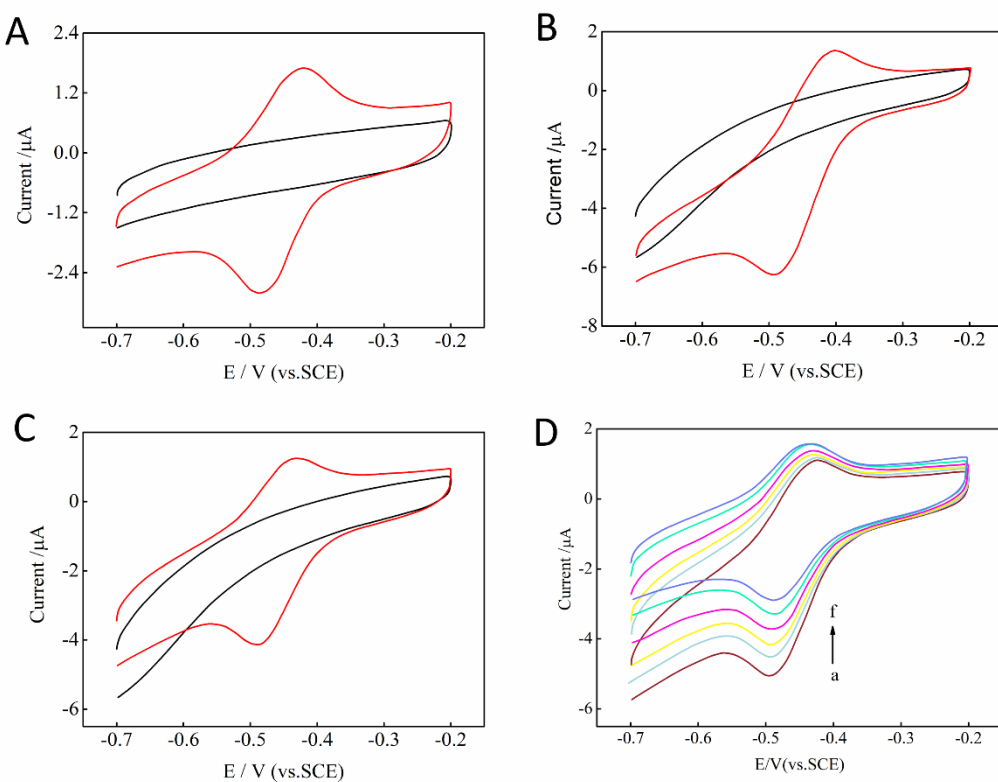


Figure 5. (A and B)Cyclic voltammograms of TiO_2/GCE (black line) and $\text{GO}_X\text{-TiO}_2/\text{GCE}$ (red line) in $0.1\text{ M PH 7.0 N}_2\text{-saturated PBS}$ and air-saturated PBS, (C) air-saturated PBS including 0.5 mM Glucose at s scan rate of 100mVs^{-1} , (D) Cyclic voltammograms of $\text{GO}_X\text{-TiO}_2/\text{GCE}$ including $0.1, 0.3, 0.5, 0.7, 1.0$ and 1.5 mM glucose (a-g) at a scan rate of 100 mVs^{-1} .

Fig.5 depicted the CV curves of different modified electrodes in N_2 -saturated and air-saturated PBS solution with the presence and absence of glucose ($\text{PH}=7.0$). It can be seen from Fig.5 (A and B) that there are no peaks observed on TiO_2/GCE electrode (black line). On the contrary, it was noticeable that the $\text{GO}_X\text{-TiO}_2/\text{GCE}$ electrode display a pair of sharped CV curves under the condition of N_2 -saturated and air-saturated solution, indicating a typical electrocatalytic process. Moreover, the anodic

peaks of $\text{GO}_x\text{-TiO}_2/\text{GCE}$ exhibits higher current response and cathodic peaks decreases simultaneously in air-saturated PBS solution compare with that of the N_2 -saturated PBS solution, reflecting dissolved oxygen was catalytically reduced at the modified electrode according to the following equations [35].

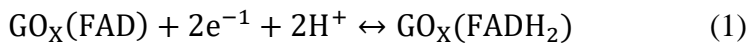


Fig.5C shows the CV curves of $\text{GO}_x\text{-TiO}_2/\text{GCE}$ by adding glucose to air-saturated PBS solution. the reduction peaks decreased compared with that of pure air-saturated PBS solution (Fig.5B) since the glucose restrained the electrocatalytic reaction attributed to the enzyme-catalyzed reaction [20]:



In addition, no peak was observed from the TiO_2/GCE electrode, all results indicating the prepared hollow spheres TiO_2 is beneficial to construct glucose biosensor. The influence of glucose concentration for electrochemical response of $\text{GO}_x\text{-TiO}_2/\text{GCE}$ has been studied in air-saturated solution displayed in Fig.5D. It showed that the reduction current response decreased correspondingly with increasing the concentration of glucose, which is possibly attribute to glucose oxidation also occurring through $\text{GO}_x\text{-FAD}/\text{GO}_x\text{-FADH}_2$ reaction centers [36].

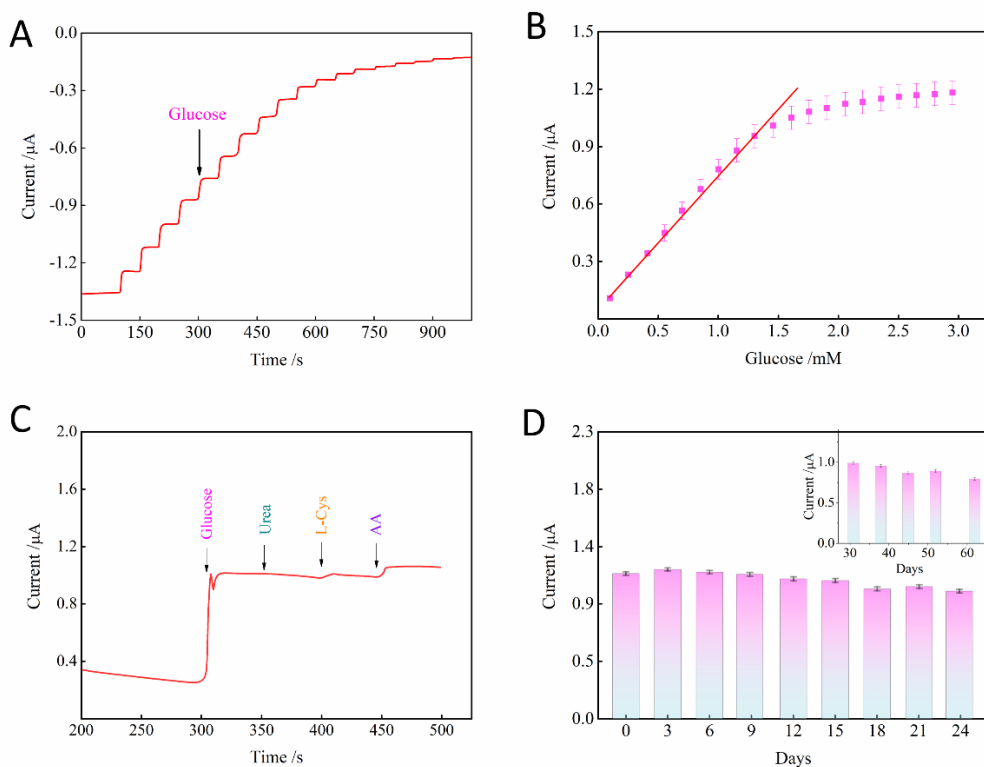


Figure 6. (A) Current-time curve of a $\text{GO}_x\text{-TiO}_2/\text{GCE}$ for successive addition of 0.1 mM of glucose to 0.1M of air-saturated PBS. (B) the calibration curve of TiO_2 modified electrode for glucose. (C) Influences of interfering species to the response of the biosensor. (D) the current response of the constructed biosensor.

The glucose sensing ability of $\text{GO}_x\text{-TiO}_2/\text{GCE}$ was investigated by measuring the change of current response with the addition of glucose in the air-saturated PBS solution. As shown in Fig.6A, the amperometric current of $\text{GO}_x\text{-TiO}_2/\text{GCE}$ electrode was obtained by successively injecting 0.1 mM Glucose at -0.45 V with a time interval of 50s. It can be obtained that the amperometric current of electrode achieved steady state current within 3s, indicating the fast current response behavior. The calibration plot from the curve of current-time depicted in Fig.6B, which displayed the linear range between 0.1 and 1.2 mM and the sensitivity was calculated to be $5.64 \mu\text{AmM}^{-1}\text{cm}^{-2}$, all results above confirmed the prepared TiO_2 gives advantages to fabricating glucose biosensor and its properties are superior to that of other nanomaterials shown in Table 1.

Table 1. Comparison of performance of some biosensor based nanomaterials

Electrode materials	Linear range (mM)	Sensitivity ($\mu\text{AmM}^{-1}\text{cm}^{-2}$)	Response time(s)	References
GO_x/TiO_2 hollow spheres	0.1~1.2	5.64	< 3	This work
GO_x/NiO hollow spheres	1.5~7	3.4	~8	[36]
$\text{GO}_x/\text{nanocrystal TiO}_2$	0~3	4.6	<30	[37]
$\text{GO}_x/\text{mesoporous TiO}_2$	0.15~1.2	3.9	<10	[19]
SPCE/CoPC/GOD	0.2~5	1.12	60	[38]
{ $\text{GO}_x/\text{Au-(SH)PANI-g-MWNT}$ }n/ITO	1~9	3.97	8	[39]
GCE-CoPc-(CoTPP)4-GO _x	~11	0.024	<5	[40]

The anti-interference performance of TiO_2 biosensors was estimated by adding interferential species containing ascorbic acid (AA), l-cysteine (l-Cys) and urea, which exists in the blood and can give rise to interfering electrochemical signals. As shown in Fig. 6C, when injecting 0.5 mM urea into air-saturated PBS solution containing 1.0 mM glucose, the current response of glucose biosensor has no obvious change and just 2.0% current changed is observed for the addition of 0.5 mM l-Cys compared with that of 1.0 mM glucose. However, the introduce of 0.5 mM AA resulted in 9.0% current increment. Considering that the 0.5 mM AA is much lower than the concentration of glucose (normal value from 4 to 7 mM in the blood); hence, it just brings about feeble interfering signals and no influence in detection of glucose. All results above confirmed that interferences species displayed negligible effect for the current response, indicating that TiO_2 biosensor possesses outstanding selectivity for determination of glucose in the blood.

To assess reproducibility of TiO_2 biosensor, current responses of fabricated biosensor was also investigated in (pH=7.0) 15 ml PBS solution with 1 mM glucose every few days. Six TiO_2/GCE electrodes were used to study the current response of glucose and relative standard deviation (RSD) of amperometric current was calculated to be 8.6%. Meanwhile, for one of fabricated glucose biosensors, the (RSD) of amperometric current of 3.2% was obtained by 15 testing successively. In addition, the long-term stability of TiO_2 biosensor was also confirmed by detecting the current response in different period time. As shown from Fig.6D, the current response of TiO_2 -modified biosensor maximized during three days and then reduced slightly. However, it retained the 85% of its initial current after three weeks and maintain 70% of that over a storage period of two months (inset plot of Fig.6D). All

results indicate that TiO₂-modified biosensor have an excellent selectivity and long-time stability, which is attribute to specific structure, bio-compatibility of TiO₂ hollow spheres as well as strong electrostatic interaction between GO_X and TiO₂ hollow spheres.

To evaluate the practicality of the GO_X-TiO₂/GCE electrode, we selected the glucose in human blood serum for testing. Human blood serum was collected from hospitalized patients and the glucose concentration was pre-determined to be 5.1 mM by a ROCHE COBAS C 111 analyzer, with 1 mL of serum was diluted to 10 mL by adding PBS (pH 7.0). The glucose in human blood serum samples were determined using GO_X-TiO₂/GCE by amperometry. The comparison of the added values and the determined values were listed in Table 2. The added glucose shows the good recoveries to 99.7% of GO_X-TiO₂/GCE. The good recoveries achieved in glucose reveal the appreciable practicality of the GO_X-TiO₂/GCE sensor. Thus, the above results reveal excellent practical feasibility of the prepared GO_X-TiO₂/GCE sensor for the determination of glucose.

Table 2. Determination of glucose in human serum samples with GO_X-TiO₂/GCE

Samples	Added(mM)	Found(mM)	RSD (%)	Recovery (%)
Bare GCE	0.5	0.687	3.5	95.2
TiO ₂ -GCE	0.5	0.756	3.2	98.5
GO _X /TiO ₂ -GCE	0.5	0.789	2.0	99.7

4. CONCLUSIONS

In summary, hollow spheres TiO₂ was fabricated by a simple and straight forward method on carbonaceous spheres. Characterization studies confirm that the hollow spheres TiO₂ give advantages to adsorb the GO_X and enhances the electron transfer between GO_X and modified electrode due to its large specific surface area and narrow pore distribution. Meanwhile, the GO_X immobilized on the TiO₂ spheres still contains its bioactivity and excellent properties, such as the large sensitivity of 5.64 $\mu\text{AmM}^{-1}\text{cm}^{-2}$, shorter response time as well as the wide linear range that is up to 1.2 mM. Most importantly, the biosensor based on the TiO₂ hollow spheres possess outstanding selectivity for determination of glucose in the blood and exhibited a long-time stability. The current response of TiO₂-modified retained the 89% of its initial current after three weeks and still maintain 70% of that over a storage period of two months. Therefore, the TiO₂ hollow spheres is seen as a promising nanomaterial to developing novel biosensors.

ACKNOWLEDGEMENTS

The authors gratefully acknowledge financial support from the National Nature Science Foundation of China (Grant Nos. No. 51661014), and Open Fund (Grant No.KKF0201928101) supported by State Key Laboratory of New Technology for Comprehensive Utilization of Rare and Precious Metals, China.

References

1. B. Liang, X. Guo, L. Fang, Y. Hu, G. Yang, Q. Zhu and X. Ye, *Electrochim. Commun.*, 50 (2015) 1-5.
2. P.N. artlett and F.A. Al-Lolage, *J. Electroanal. Chem.*, 819 (2018) 26-37.
3. T. Terse-Thakoor, K. Komori, P. Ramnani, I. Lee and A. Mulchandani, *Langmuir*, 31 (2015) 13054-13061.
4. E. Arango Gutierrez, A.M. Wallraf, A. Balaceanu, M. Bocola, M.D. Davari, T. Meier and U. Schwaneberg, *Biotechnol. Bioeng.*, 115 (2018) 2405-2415.
5. R. Zhao, X. Liu, J. Zhang, J. Zhu and D.K. Wong, *Electrochim. Acta*, 163(2015), 64-70.
6. C.X. Guo, and C.M. Li, *Phys. Chem. Chem. Phys.*, 12 (2010) 12153-12159
7. Q. Guo, L. Liu, M. Zhang, H. Hou, Y. Song, H. Wang and L. Wang, *Biosens. Bioelectron.*, 92 (2017) 654-660.
8. J. Kim, A.S Campbell and J. Wang, *Talanta*, 177 (2018) 163-170.
9. Q. Liu, Y. Liu, F. Wu, X. Cao, Z. Li, M. Alharbi and C. Zhou, *ACS Nano*, 12 (2018) 1170-1178.
10. Z. Wang, S. Liu, P. Wu and C. Cai, *Anal. Chem.*, 81 (2009) 1638-1645.
11. J.M. Goran, S.M. Mantilla and K. Stevenson, *Anal. Chem.*, 85 (2013) 1571-1581.
12. X. Yang, Q. Bi, H. Ali, K. Davis, W. Schoenfeld and K. Weber, *Adv. Mater.*, 28 (2016) 5891-5897.
13. M. Barawi, L. DeTrizio, R. Giannuzzi, G. Veramonti, L. Manna, and M. Manca, *ACS Nano*, 11 (2017) 3576-3584.
14. D.H. Lee, B.H. Lee, A.K. Sinha, J.H. Park, M.S. Kim, J. Park, and T. Hyeon, *J. Am. Chem. Soc.*, 140 (2018) 16676-16684.
15. J. Zhang, X. Yu, W. Guo, J. Qiu, X. Mou, A. Li and H. Liu, *Nanoscale*, 8 (2016) 9382-9389.
16. T.P. Tsele, A.S. Adekunle, O.E. Fayemi and E.E. Ebenso, *Electrochim. Acta*, 243 (2017) 331-348.
17. C. Zhang, S. Si and Z. Yang, *Biosens. Bioelectron.*, 65 (2015) 115-120.
18. Q. Yang, C. Yang, Q. Wang, F. Yang, C. Song and H. Yang, *J. Electrochem. Soc.*, 165 (2018) B610-B615.
19. S.J. Bao, C.M. Li, J.F. Zang, X.Q. Cui, Y. Qiao and J. Guo, *Adv. Funct. Mater.*, 18 (2008) 591-599.
20. Z. Yang, Y. Tang, J. Li, Y. Zhang and X. Hu, *Biosens. Bioelectron.*, 54 (2014) 528-533.
21. J. Tang, Y. Wang, J. Li, P. Da, J. Geng and G. Zheng, *J. Mater. Chem. A.*, 2 (2014) 6153-6157.
22. W.R. Hendren, A. Murphy, P. Evans, D. O'Connor, G.A. Wurtz, A.V. Zayats, and R.J. Pollard, *J. Phys-Condens. Mat.*, 20 (2008) 362203.
23. I. Yamaguchi, M. Watanabe, T. Shinagawa, M. Chigane, M. Inaba, A. Tasaka and M. Izaki, *ACS Appl. Mater. Inter.*, 1 (2009) 1070-1075.
24. A.A. Ensafi, N.Ahmadi and B. Rezaei, *Sensor. Actuat. B-Chem.*, 239 (2017) 807-815.
25. D. Liu, X. Zhang and T. You, *ACS Appl. Mater. Inter.*, 6 (2014) 6275-6280.
26. H. Liu, Y. Tian and Z. Deng, *Langmuir*, 23 (2007) 9487-9494.
27. S.J. Bao, C.M. L, J.F. Zang, X.Q. Cui, Y. Qiao and J. Guo, *Adv. Funct. Mater.*, 18 (2008) 591-599.
28. E. Laviron, *J. Electroanal. Chem. Inter. Electrochem.*, 101 (1979) 19-28.
29. M.V. Jose, S. Marx, H. Murata, R.R. Koepsel and A.J. Russell, *Carbon*, 50 (2012) 4010-4020.
30. J. Liu, A. Chou, W. Rahmat, M.N. Paddon-Row and J.J. Gooding, *Electroanal.*, 17 (2005) 38-46.
31. H. Zhang, Z. Meng, Q. Wang and J. Zheng, *Sensor. Actuat. B-Chem.*, 158 (2011) 23-27.
32. H. Liu, W. Li, D. Shen, D. Zhao and G. Wang, *J. Am. Chem. Soc.*, 137 (2015) 13161-13166.
33. Y. Zhang, Y. Zhao, S. Cao, Z. Yin, L. Cheng and L. Wu, *ACS Appl. Mater. Inter.*, 9 (2017) 29982-29991.
34. J. Wang, Y. Bai, M. Wu, J. Yin and W. Zhang, *J. Power Sources*, 191 (2009) 614-618.
35. J. Liu, C. Guo, C.M. Li, Y. Li, Q. Chi, X. Huang and T. Yu, *Electrochim. Commun.*, 11 (2009) 202-205.
36. C.X. Guo and C.M. Li, *Phys. Chem. Chem. Phys.*, 12 (2010) 12153-12159.

37. Q. Li, G. Luo, J. Feng, Q. Zhou, L.I. Zhang and Y. Zhu, *Electroanal.*, 13 (2001) 413-416.
38. E. Crouch, D.C. Cowell, S. Hoskins, R.W. Pittson and J.P. Hart, *Anal. Biochem.*, 347 (2005) 17-23.
39. S. Komathi, A.I. Gopalan and K.P. Lee, *Biosens. Bioelectron.*, 24 (2009) 3131-3134.
40. K.I. Ozoemena and T. Nyokong, *Electrochim. Acta*, 51 (2006) 5131-5136.

© 2020 The Authors. Published by ESG (www.electrochemsci.org). This article is an open access article distributed under the terms and conditions of the Creative Commons Attribution license (<http://creativecommons.org/licenses/by/4.0/>).